Review of Scientific Instruments

RESEARCH ARTICLE | NOVEMBER 22 2017

A large ion beam device for laboratory solar wind studies

Zach Ulibarri; Jia Han; Mihály Horányi; Tobin Munsat; Xu Wang ; Guy Whittall-Scherfee; Li Hsia Yeo

Check for updates

Rev. Sci. Instrum. 88, 115112 (2017)
https://doi.org/10.1063/1.5011785

View Online
Export Citation

Articles You May Be Interested In

Full kinetic simulations of plasma flow interactions with meso- and microscale magnetic dipoles

Phys. Plasmas (December 2014)

Laboratory plasma devices for space physics investigation

Rev. Sci. Instrum. (July 2021)

Fore-wake excitations from moving charged objects in a complex plasma

Phys. Plasmas (October 2016)

19 June 2026 00:46:47

AIP Advances
Why Publish With Us?
21DAYS average time to 1st decision
OVER 4 MILLION views in the last year
INCLUSIVE scope
Learn More
AIP Publishing

AIP Publishing

A large ion beam device for laboratory solar wind studies

Zach Ulibarri,[1,2,a)] Jia Han,[1,2] Mihály Horányi,[1,2] Tobin Munsat,[1,2] Xu Wang,[1] Guy Whittall-Scherfee,[3] and Li Hsia Yeo[1,2]
[1]*Institute for Modeling Plasma, Atmospheres and Cosmic Dust (IMPACT), University of Colorado, Boulder, Colorado 80309, USA*
[2]*Department of Physics, University of Colorado, Boulder, Colorado 80309, USA*
[3]*Department of Physics, St. Mary's College, Moraga, California 94556, USA*

(Received 22 December 2016; accepted 1 November 2017; published online 22 November 2017)

The Colorado Solar Wind Experiment is a new device constructed at the Institute for Modeling Plasma, Atmospheres, and Cosmic Dust at the University of Colorado. A large cross-sectional Kaufman ion source is used to create steady state plasma flow to model the solar wind in an experimental vacuum chamber. The plasma beam has a diameter of 12 cm at the source, ion energies of up to 1 keV, and ion flows of up to 0.1 mA/cm^2. Chamber pressure can be reduced to 4×10^{-5} Torr under operating conditions to suppress ion-neutral collisions and create a monoenergetic ion beam. The beam profile has been characterized by a Langmuir probe and an ion energy analyzer mounted on a two-dimensional translation stage. The beam profile meets the requirements for planned experiments that will study solar wind interaction with lunar magnetic anomalies, the charging and dynamics of dust in the solar wind, plasma wakes and refilling, and the wakes of topographic features such as craters or boulders. This article describes the technical details of the device, initial operation and beam characterization, and the planned experiments. *Published by AIP Publishing.* https://doi.org/10.1063/1.5011785

I. INTRODUCTION

Airless planetary bodies, such as asteroids, dormant comets, and most moons, have no significant atmospheres or global magnetic fields and therefore have surfaces that are directly exposed to the solar wind plasma. Recent *in situ* observations on the lunar surface have shown that solar wind bombardment generates several physical processes on the upstream side. These processes include reflected and backscattered solar wind ions,[1] neutral atoms backscattered by charge-exchange at the lunar surface,[2,3] and sputtering products.

On the downstream side, a distinct physical feature, plasma wakes (or voids) are formed. These wakes have much lower electron and ion densities than the bulk flow of the solar wind. Because thermal electrons have higher mobility than the supersonic ions, they move into the wakes first, resulting in charge separation near the wake boundaries. Ambipolar electric fields form and accelerate the ions into the wake regions. Complicated physical phenomena are created in the wake region,[4] including ion acceleration, rarefaction waves that propagate into the ambient undisturbed plasmas, excitation of plasma oscillations and instabilities, and strong plasma discontinuities at the expansion front. The lunar plasma wake has been widely investigated by computer simulations and *in situ* observations,[5] and while there have been advances in our understanding of the refilling process,[6] there is a lack of fully controlled laboratory experiments addressing wake formation in steady flowing plasmas which are necessary to corroborate these theoretical results. Few laboratory experiments have been performed to study wake formation behind planetary bodies in the solar wind, and even these were investigated using pulsed plasma sources.[7–10] Further, the wake behind moons, asteroids, and even spacecraft is still being investigated, and laboratory experiments will further elucidate the results of these missions.

Recently, the plasma wakes created by smaller airless bodies such as asteroids and comets have attracted greater attention due to the increase in space missions investigating such bodies.[11,12] We aim to investigate the plasma wakes formed at obstacles of various sizes (relative to the Debye length) and shapes using laboratory experiments with more realistic solar wind plasma conditions than any attempted thus far.

Additionally, interactions between the solar wind plasma and localized features on the surface of airless bodies also generate interesting physical processes and phenomena. Studies have shown that the magnetic anomalies on the lunar surface (e.g., crustal magnetic fields) have a strong influence on the incoming solar wind plasma, and this results in deflection/reflection of the solar wind ions,[13] the formation of mini-magnetospheres,[14–18] and possibly large positive surface potentials.[19–22] More interestingly, the high-albedo swirl-shaped markings observed on the lunar surface have been found to show a strong correlation with lunar magnetic anomalies and their interaction with the solar wind plasma.[23] Previously we have experimentally studied the dynamics of charged particles and electrostatic environments at a surface embedded in a magnetic dipole field with non-flowing plasmas[24,25] and flowing plasmas with low ion energies.[21] The Colorado Solar Wind Experiment (CSWE) marks an upgrade to our laboratory studies that allows for realistic solar wind plasma conditions. When the solar wind flows over topographical features on the

a)zachary.ulibarri@colorado.edu

19 June 2026 00:46:47

planetary surfaces (e.g., craters or large boulders), the process of plasma expansion into the craters or the downstream side boulders differs from the global-scale plasma wakes due to the effects of the electric fields formed at the surface. Electric environments at the topographical surfaces have been mainly studied using computer simulations[26,27] and have only been recently investigated with laboratory experiments.[28]

Plasma-dust interaction has been an important topic for decades, as this determines the dynamics of cometary dust tails, dust exospheres, and interplanetary dust.[29,30] Electrostatic dust transport on the surfaces of airless planetary bodies has been suggested to explain a variety of unusual planetary phenomena.[31–35] Our recent experiments have shown that the emission and re-absorption of photo-electrons and/or secondary electrons at rough dusty surfaces are responsible for the initial mobilization and launch of regolith dust particles.[36] However, while dust charging and dynamics in thermal plasma conditions have been investigated,[37–45] these dynamics have not been studied under solar wind conditions in laboratory experiments.[28]

In summary, many new physical processes have been observed *in situ* and through computer simulations, but these need to be combined with laboratory experiments to answer remaining questions. We have constructed the CSWE at the Institute for Modeling Plasma, Atmospheres, and Cosmic Dust (IMPACT) to advance our understanding of the solar wind interaction with airless planetary bodies and dust. This device is unique due to its steady state plasma flow with a large cross section (greater than 12 cm in diameter) that allows for measurement using probes, high ion energy (up to 1 keV, a typical solar wind ion energy), and large ion flux (up to 0.1 mA/cm^2). This is in contrast to pulsed plasmas or steady state flows with small cross sections mostly used in previous laboratory experiments. This paper describes the performance of the CSWE and the planned experiments.

II. ION SOURCE AND VACUUM SYSTEMS

The CSWE consists of a large aperture (12 cm in diameter) high-current Kaufman KDC 100 ion source attached to an experimental vacuum chamber 183 cm in length and 76 cm in diameter. A picture of the chamber is shown in Fig. 1, and a diagram of the ion source is shown in Fig. 2. Gas, such as nitrogen or argon, flows into the ion source where it is ionized by energetic electrons emitted from a heated cathode. Ions created

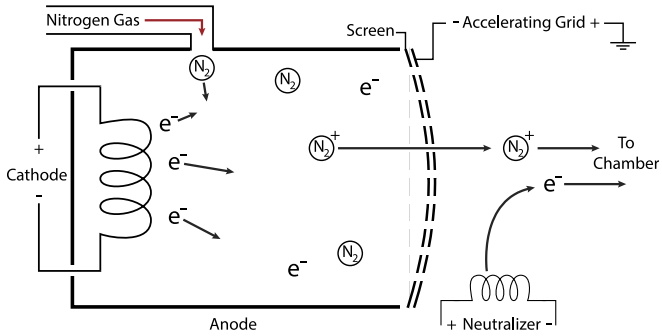

FIG. 2. A diagram of the CSWE ion source. Nitrogen gas is ionized by energetic electrons emitted from a hot cathode. Ions are extracted through a screen grid by a negatively biased accelerating grid. Curvature of these grids diverges the beam to increase its cross section and uniformity. A hot filament neutralizer supplies electrons to maintain quasi-neutrality of the flowing plasma.

in the source are extracted by a negatively biased accelerating grid through a screen grid into the chamber. The ion energy is selected by the anode potential with respect to ground (i.e., the ion energy is the value of the anode potential in eV). Curvature of the grids creates an ion optics system that diverges the ion flow by 7° to increase the beam cross section and uniformity in the experimental chamber. A neutralizing filament located at the exit of the source is used to maintain quasi-neutrality of the flowing plasma.

Since the gas flowing into the ion source will build up pressure in the experimental chamber and cause ion-neutral collisions (charge-exchange), a differential pressure chamber backed by a turbo-molecular pump isolates the ion source from the rest of the chamber, which is in turn backed by two diffusion pumps. The chamber itself has a base pressure of 3×10^{-7} Torr and an operating pressure of 4×10^{-5} Torr.

The CSWE has been tested using hydrogen, nitrogen, and argon. While hydrogen is the best analog for the solar wind, its low ionization cross section requires higher gas flows in order to achieve desired currents. This results in a higher degree of charge-exchange, limiting the observed flux of high velocity ions in the experimental chamber. Nitrogen and argon, however, can be ionized at a low pressure without significant charge-exchange collisions. For the characterization presented here, the CSWE used N_2^+ because it has a lower mass than argon.

Depending on the purpose of investigations being performed when studying the solar wind interaction with airless

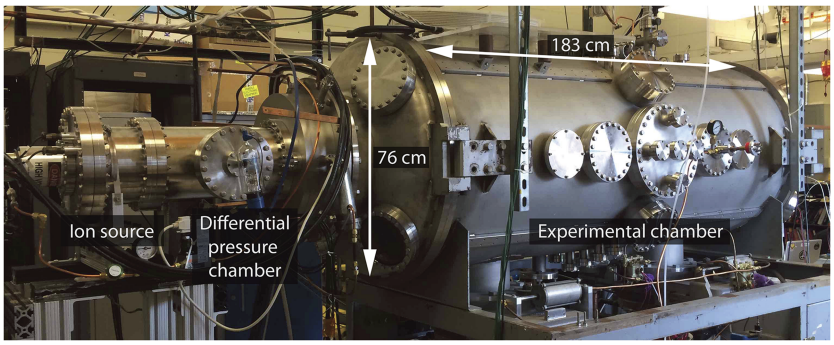

FIG. 1. A photo of the CSWE chamber. Ionized gas is created in the ion source, and an accelerating potential pulls the ions into the experimental chamber. A differential pressure chamber prevents excess gas buildup in the experimental chamber.

19 June 2026 00:46:47

surfaces, a variety of different types of ion sources may be used. For example, ion sources with small apertures (i.e., small cross-sectional plasma flow) are often used to study how surface processes such as sputtering and space weathering are sustained by solar wind bombardment. To study the physical processes of solar wind interaction with airless bodies, however, we require a large cross-sectional area of plasma flow (that is, a large aperture ion source) to allow access for probe measurements and to immerse the targets in the plasma flow. This large aperture necessarily reduces the effectiveness of differential pumping, resulting in a certain degree of ion-neutral charge-exchange collisions that create a population of thermal ions, a feature not present in the solar wind.

The KDC 100 ion source has a sophisticated set of ion optics which focus the flowing ions into a coherent beam. These optics are designed to operate within a specific parameter space as they become more or less efficient depending on the ion current and accelerating potential settings. For example, the source is not designed to supply large currents at low voltages (such as 80 mA of ion current with a beam energy of 200 eV). For this reason, when the ion current is doubled, the measured ion flux may not be doubled.

III. DIAGNOSTICS

The parameters of the plasma produced in the CSWE are measured by a double planar Langmuir probe, which consists of two tantalum discs 6.35 mm in diameter with an insulating layer between them. With this probe, the plasma potential, the electron density, and the electron temperature are measured.

An Ion Energy Analyzer (IEA) is used to measure the ion energy and flux.[46] This instrument uses retarding fields to measure the distribution of ion energies. Sample traces from the IEA are shown in Fig. 3. There is a sharp falloff at each selected energy, indicating that the beam energy is highly mono-energetic.

The double Langmuir probe and IEA are mounted on a 2-axis translation stage controllable from outside the vacuum chamber that allows them to be moved around the chamber

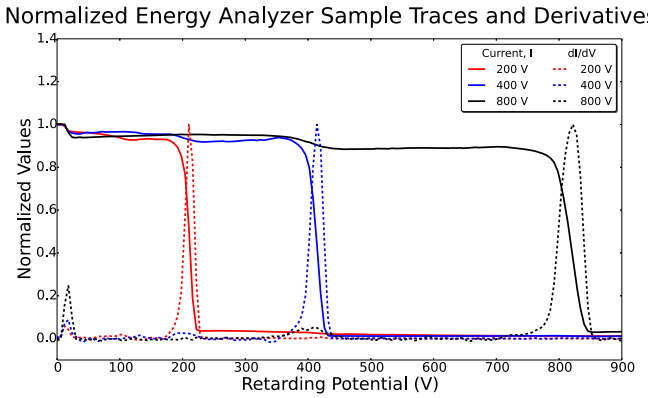

FIG. 3. Sample traces from the Ion Energy Analyzer (IEA) showing measured ion current as a function of retarding potential for three different ion energies. Solid lines denote the measured current, while dotted lines denote the derivative. There is a sharp drop at each specified energy, indicating that the flow is highly uniform in its velocity distribution.

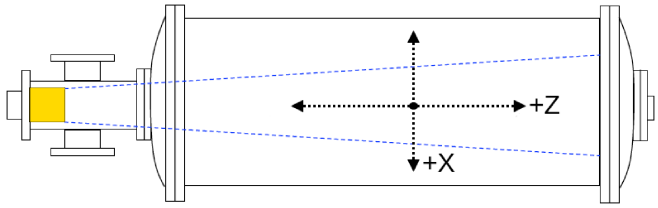

FIG. 4. A top-down diagram of the coordinates used in the CSWE. The X-axis measures the horizontal displacement from the beam's center axis, while the Z-axis measures the distance from the source itself.

to map out the plasma parameters in a 2D profile. Positions of the probe measurements are mapped according to the axes defined in Fig. 4.

IV. PERFORMANCE

A comparison of plasma parameters between space and laboratory conditions is summarized in Table I. While the CSWE is capable of achieving the typical solar wind ion energy of 1 keV, the mass of N_2^+ is heaver than that of a proton, resulting in a slower ion velocity. The ion Mach number, however, which is the ratio of the ion flow speed to the ion sound speed, is the dominant term in the ion flow characterization. In both space and laboratory conditions, it is much larger than 1 (indicating supersonic flow). We note that the beam ion temperature has been used to calculate the ion sound speed since it is much larger than the dominant electron temperature. It is impossible and unnecessary to attain the same order of magnitude of either the density or the Debye length of the solar wind in laboratory settings. However, the dimensionless Debye ratio, which is the ratio of the Debye length to the size of an object, has more physical meaning when studying plasma interaction with objects. Planned experiments include inserting objects up to 10 cm in diameter into the plasma beam. Since the CSWE can be used to create Debye lengths of 0.2 cm, the CSWE Debye ratio has a lower limit of 0.02. The Debye ratio is therefore $\ll 1$, which is typical for many features of interest (for example, craters on the lunar surface, where the Debye length is on the order of 10 m). Thus, the CSWE will provide accurate simulation of plasma processes in these regions.

TABLE I. Comparison of parameters between space and laboratory conditions. The ion Mach number measures the ratio of the plasma's flow speed to its sound speed. The Debye ratio is the ratio of the Debye length to the characteristic scales of experimental features (e.g., simulated craters or other surface topography).

	Solar wind	Laboratory
Velocity, v_i	450 km/s	83 km/s
Ion energy	1 keV	1 keV
Ion species	H^+	N_2^+
Electron temperature, T_e	10 eV	0.5 eV (cold) 10 eV (hot)
Ion temperature, T_i	10 eV	14 eV
Ion Mach number, $\frac{v_i}{(T_i/m_i)^{1/2}}$	**9**	**11**
Density, n	$10\ cm^{-3}$	10^7–$10^8\ cm^{-3}$
Debye length, λ_d	10^3 cm	0.2 cm
Debye ratio, λ_d/L (L is the dimension of an object)	$\ll 1$	$\ll 1$ (minimum 0.02)

19 June 2026 00:46:47

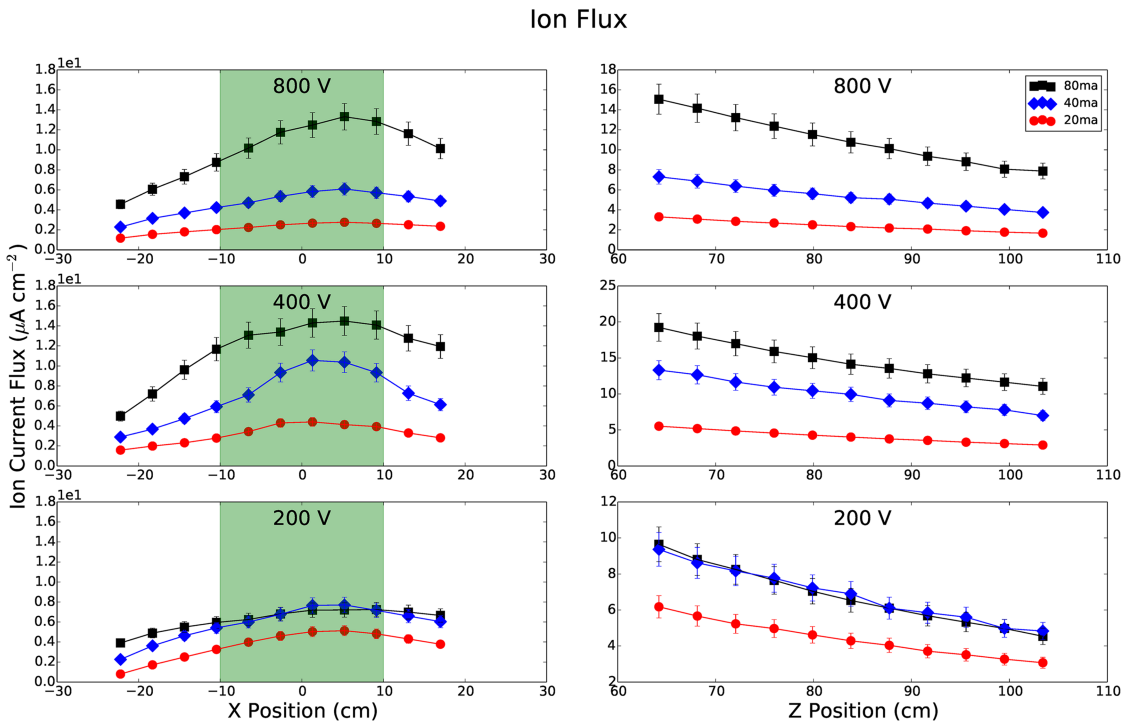

FIG. 5. Plots of the particle flux for each position on the x and z axes. These values were calculated from the IEA measurements. The green shaded region denotes the designated experimental region. Note that the flux at 80 mA and 200 V is lower than the flux at 40 mA.

Figure 5 shows results from the IEA as a function of position in both X and Z. The green shaded region denotes the designated experimental region, while data points outside this space were investigated for completeness. Over the experimental region, the uniformity of the ion flux and electron density is around 30%. In general, the source behaves as expected except for the 200 eV 80 mA ion flow, in that the flux roughly doubles when the source current is doubled. The

19 June 2026 00:46:47

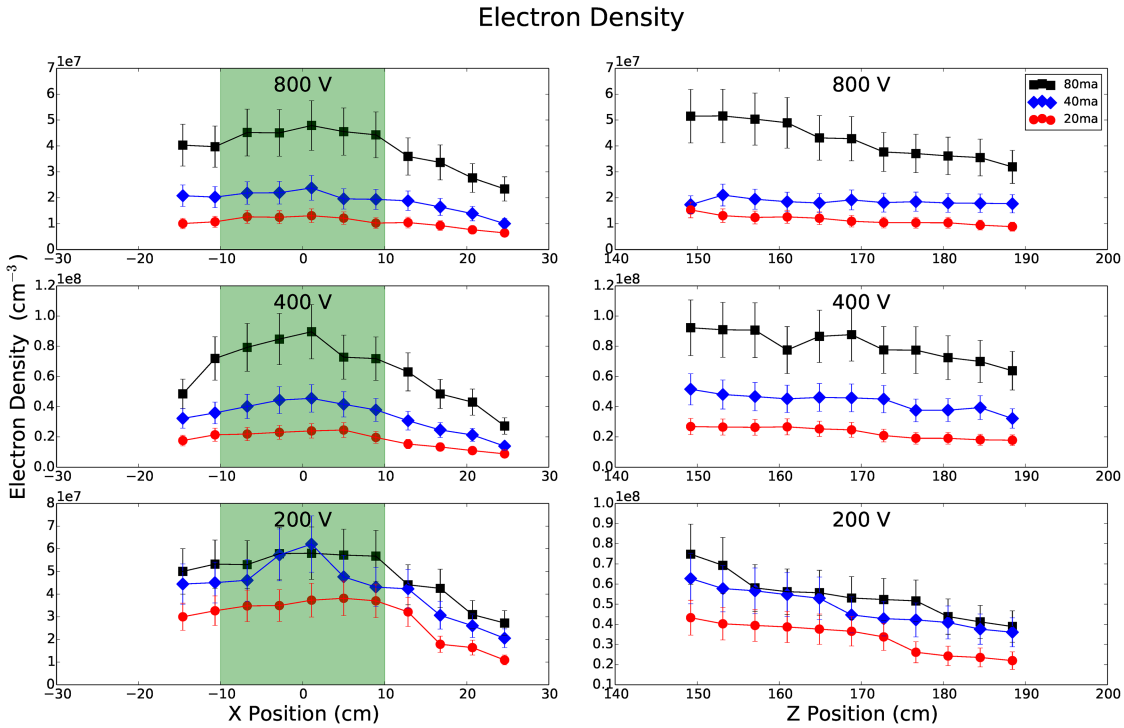

FIG. 6. Plots of the electron density for each position on the x and z axes. These values were analyzed from the Langmuir probe measurements. The green shaded region denotes the designated experimental space.

current density peaks in the center of the beam and drops as the distance from the source increases.

At 200 V anode potential, the flux from 80 mA is lower than that of 40 mA. This occurs because of the efficiency of the source's ion optics, which is discussed in Sec. II. When operating with these parameters, the current through the accelerating grid in the source is an order of magnitude higher than that at other settings, indicating that a significant fraction of the ions collide with the grid and are thus never flowed into the chamber. This provides a lower bound for the anode voltage when operating at high currents. Similarly, the 800 V, 80 mA ion flux is greater in magnitude than expected, and this is likely due to increased performance of the ion optics in this parameter region.

Figure 6 shows the electron density as measured by the Langmuir probe. Two Maxwellian distributions of electrons are observed in the Langmuir probe current-voltage (I-V) characteristics, with the hot population having a temperature of around 10 eV and density that is approximately 1% of that of the cold population, which have temperatures near 0.5 eV. The plot shown in Fig. 6 includes both of these populations. Bi-Maxwellian electron populations often exist in hot-cathode generated plasmas. Hot electrons may be caused by primary electrons that carry the remaining energies after the ionization of neutral particles. Secondary electrons induced by the bombardment of primary electrons or beam ions on the chamber walls may also create such hot electrons.[47] The exact mechanisms remain unclear.

The solar wind ions have a supersonic flow speed with a thermal temperature of about 10 eV. I-V characteristics from the IEA were used to find the temperature of the beam ions. As described in Sec. II, the CSWE produces thermal ions in addition to supersonic ions due to charge-exchange collisions. Although the flux of flowing ions dominates the thermal ion flux, the density of thermal ions is not negligible. The ratio of the beam to thermal ion densities is shown in Fig. 7. Their densities were calculated by dividing the measured fluxes of ions at beam and thermal energies by the speeds at these energies. The ratio is close to one for 800 eV ions, and as high as two for lower ion energies. Thus, the effect of thermal ions on wake and surface topography experiments needs to be taken into account. For investigations of magnetic anomalies or dust charging and dynamics, the flux is a more important parameter than the density. The effect of thermal ions will therefore be less pronounced in these experiments.

V. PLANNED EXPERIMENTS

The planned experiments are schematically illustrated in Fig. 8 and detailed below.

A. Solar wind interaction with magnetic anomalies

This topic has been extensively studied recently as described in the Introduction. However, most of the available *in situ* space observations addressed the dynamics of particles and fields at high altitudes. We will upgrade our previous laboratory studies[24,25] from low-energy (<50 eV) to high-energy (1 keV) ion flow to investigate the electric environments at the surface in magnetic anomaly regions, which have important consequences for understanding various surface processes, such as space weathering and electrostatic dust transport. The ion inertial length, d_i, is an important parameter in the charge separation process associated with solar wind

19 June 2026 00:46:47

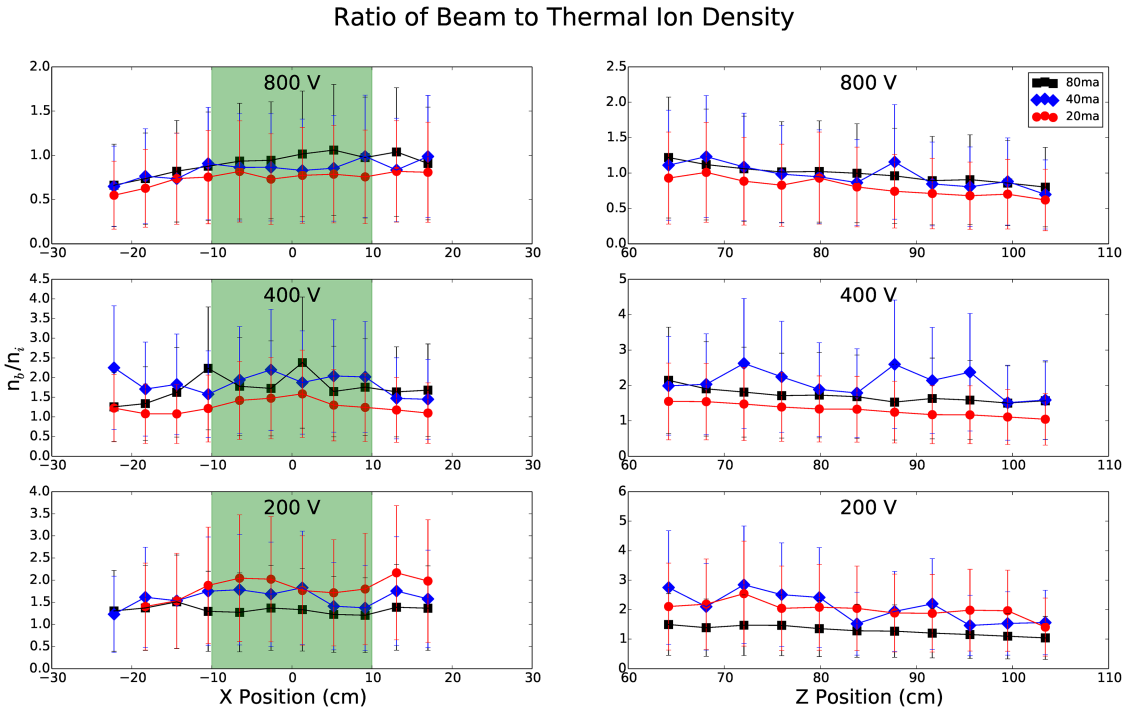

FIG. 7. Plots of the ratio of beam to thermal ion density for each position on the x and z axes. These values were calculated from the IEA measurements.

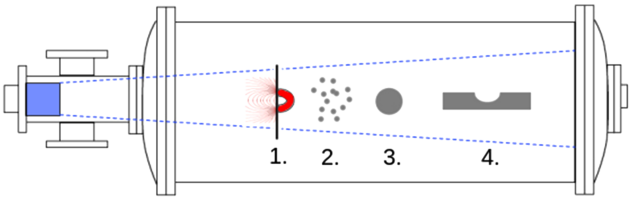

FIG. 8. A diagram of the planned experiments. 1. Solar wind interaction with magnetic anomalies. 2. Dust charging and dynamics. 3. Plasma wakes. 4. Topographical wakes.

interaction with lunar magnetic anomalies. On the lunar surface, d_i is similar to or larger than the characteristic scale of magnetic anomalies.[16] However, the ion inertial length in the CSWE is on the order of a few hundred meters, much larger than CSWE experimental magnetic field length scales. The CSWE studies cases when ions penetrate the dipole field to impact the surface, as has been indicated from observations using the neutral atom energy spectrometer SARA/CENA on Chandrayaan-1.[19]

B. Charging and dynamics of dust in the solar wind

Charging of dust particles exposed to non-flowing plasmas has been extensively studied, but the CSWE will allow us to study dust charging and dynamics in flowing plasmas with a variety of ion flow speeds. Additionally, interaction of solar wind with dust clouds (e.g., dust exospheres around planetary bodies) will be investigated.

C. Plasma wakes

Wake experiments will be performed by inserting objects as large as 10 cm in diameter in the simulated solar wind. The large cross-sectional plasma flow will allow probe diagnosis possible in the wake regions to unravel the dynamics of the electron and ion refilling of the wake. We will map the spatial profiles of plasma parameters to measure waves and instabilities. In addition, the surface charging in the wake will be studied using a configuration of segmented surfaces with which floating potentials will be measured. We will also investigate the wake of irregular-shaped obstacles in the solar wind, such as asteroids and comets.

D. Wakes of topographic features

By inserting models of various surface features such as craters or boulders, we will measure the plasma wake effects of topographic entities. This study is particularly important for understanding the local electric environments in permanently shadowed regions, in which plasma may play a role in volatile production/loss.

VI. SUMMARY AND CONCLUSION

A new, large cross-sectional, high-current, high-energy ion source at the SSERVI IMPACT has been constructed and tested. This source will provide laboratory solar wind simulations that more accurately model realistic conditions than previous experiments involving smaller cross-sectional sources or those involving low or non-flowing plasmas. The CSWE will provide laboratory investigations of a variety of outstanding questions about solar wind interaction with airless planetary bodies, such as surface electric environment in the presence of magnetic anomalies, dust charging and dynamics, and plasma wakes resulting from airless bodies and topographical features on their surfaces.

ACKNOWLEDGMENTS

This work was supported by the NASA/SSERVI's Institute for Modeling Plasma, Atmospheres, and Cosmic Dust.

[1]Y. Saito, S. Yokota, T. Tanaka, K. Asamura, M. N. Nishino, M. Fujimoto, H. Tsunakawa, H. Shibuya, M. Matsushima, H. Shimizu, F. Takahashi, T. Mukai, and T. Tersawa, "Solar wind proton reflection at the lunar surface: Low energy ion measurement by map-pace onboard selene (kaguya)," Geophys. Res. Lett. **35**, L24205, doi:10.1029/2008GL036077 (2008).
[2]D. J. McComas, "Lunar backscatter and neutralization of the solar wind: First observations of neutral atoms from the moon," Geophys. Res. Lett. **36**, L12104, doi:10.1029/2009GL038794 (2009).
[3]A. Schaufelberger, P. Wurz, S. Barabash, M. Wieser, Y. Futaana, M. Holmstrm, A. Bhardwaj, M. B. Dhanya, R. Sridharan, and K. Asamura, "Scattering function for energetic neutral hydrogen atoms off the lunar surface," Geophys. Res. Lett. **38**, L22202, doi:10.1029/2011GL049362 (2011).
[4]U. Samir, K. H. Wright, and N. H. Stone, "The expansion of a plasma into a vacuum: Basic phenomena and processes and applications to space plasma physics," Rev. Geophys. **21**, 1631–1646, doi:10.1029/rg021i007p01631 (1983).
[5]J. S. Halekas, Y. Saito, G. T. Delory, and W. M. Farrell, "New views of the lunar plasma environment," Planet. Space Sci. **59**, 1681–1694 (2011).
[6]J. Wang and D. E. Hastings, "Ionospheric plasma flow over large high-voltage space platforms. I: Ion-plasma–time scale interactions of a plate at zero angle of attack," Phys. Fluids B **4**(6), 1597–1614 (1992).
[7]L. Kristoferson, "Laboratory simulation experiment on solar wind interaction with the moon," J. Geophys. Res. **74**(3), 906–908, doi: 10.1029/ja074i003p00906 (1969).
[8]I. M. Podgorny and Y. V. Andrijanov, "Simulation of the solar wind interaction with non-magnetic celestial bodies," Planet. Space Sci. **26**(2), 99–109 (1978).
[9]D. S. Intriligator and G. R. Steele, "Observations of structuring in the downstream region of a large spherical model in a laboratory simulated solar wind plasma," J. Geophys. Res. **87**(A8), 6053–6059, doi: 10.1029/ja087ia08p06053 (1982).
[10]D. S. Intriligator and G. R. Steele, "Analyses of experimental observations of electron temperatures in the near wake of a model in a laboratory-simulated solar wind plasma," J. Geophys. Res. **90**(A5), 4027–4034, doi: 10.1029/ja090ia05p04027 (1985).
[11]M. I. Zimmerman, W. M. Farrell, and A. R. Poppe, "Grid-free 2d plasma simulations of the complex interaction between the solar wind and small, near-earth asteroids," Icarus **238**, 77–85 (2014).
[12]T. A. Nordheim, G. H. Jones, J. S. Halekas, E. Roussos, and A. J. Coates, "Surface charging and electrostatic dust acceleration at the nucleus of comet 67p during periods of low activity," Planet. Space Sci. **119**, 24–35 (2015).
[13]C. Lue, Y. Futaana, S. Barabash, M. Wieser, M. Holmstrom, A. Bhardwaj, M. Dhanya, and P. Wurz, "Strong influence of lunar crustal fields on the solar wind flow," Geophys. Res. Lett. **38**, L03202, doi:10.1029/2010GL046215 (2011).
[14]J. S. Halekas, G. T. Delory, D. A. Brain, R. P. Lin, and D. L. Mitchell, "Density cavity observed over a strong lunar crustal magnetic anomaly in the solar wind: A mini-magnetosphere?," Planet. Space Sci. **56**, 941–946, doi:10.1016/j.pss.2008.01.008 (2008).
[15]M. Wieser, S. Barabash, Y. Futaana, M. Holmstrom, A. Bhardwaj, R. Sridharan, M. B. Dhanya, P. Wurz, A. Schaufelberger, and K. Asamura, "First observation of a mini-magnetosphere above a lunar magnetic anomaly using energetic neutral atoms," Geophys. Res. Lett. **37**, L015103, doi: 10.1029/2009GL041721 (2010).

19 June 2026 00:46:47

[16]R. A. Bamford, B. Kellett, W. J. Bradford, C. Norberg, A. Thornton, K. J. Gibson, I. A. Crawford, L. Silva, L. Gargat, and R. Bingham, "Mini-magnetospheres above the lunar surface and the formation of lunar swirls," Phys. Rev. Lett. **109**, 081101 (2012).
[17]J. Deca, A. Divin, G. Lapenta, B. Lembge, S. Markidis, and M. Horányi, "Electromagnetic particle-in-cell simulations of the solar wind interaction with lunar magnetic anomalies," Phys. Rev. Lett. **112**, 151102 (2014).
[18]J. Deca, A. Divin, B. Lembge, M. Horányi, S. Markidis, and G. Lapenta, "General mechanism and dynamics of the solar wind interaction with lunar magnetic anomalies from 3-d particle-in-cell simulations," J. Geophys. Res. **120**, 6443–6463, doi:10.1002/2015JA021070 (2015).
[19]Y. Futaana, S. Barabash, M. Wieser, C. Lue, P. Wurz, A. Vorburger, A. Bhardwaj, and K. Asamura, "Remote energetic neutral atom imaging of electric potential over a lunar magnetic anomaly," Geophys. Res. Lett. **40**, 262–266, doi:10.1002/grl.50135 (2013).
[20]R. Jarvinen, M. Alho, E. Kallio, P. Wurz, S. Barabash, and Y. Futaana, "On vertical electric fields at lunar magnetic anomalies," Geophys. Res. Lett. **41**, 2243, doi:10.1002/2014gl059788 (2014).
[21]C. T. Howes, X. Wang, J. Deca, and M. Horányi, "Laboratory investigation of lunar surface electric potentials in magnetic anomaly regions," Geophys. Res. Lett. **42**, 4280–4287, doi:10.1002/2015gl063943 (2015).
[22]M. I. Zimmerman, W. M. Farrell, and A. R. Poppe, "Kinetic simulations of kilometer-scale mini-magnetosphere formation on the moon," J. Geophys. Res.: Planets **120**, 1893–1903, doi:10.1002/2015je004865 (2015).
[23]D. T. Blewett, E. I. Coman, B. R. Hawke, J. J. Gillis-Davis, M. E. Purucker, and C. G. Hughes, "Lunar swirls: Examining crustal magnetic anomalies and space weathering trends," J. Geophys. Res. **116**, E02002, doi:10.1029/2010JE003656 (2011).
[24]X. Wang, M. Horányi, and S. Robertson, "Characteristics of a plasma sheath in a magnetic dipole field: Implications to the solar wind interaction with the lunar magnetic anomalies," J. Geophys. Res. **117**, A06226, doi:10.1029/2012JA017635 (2012).
[25]X. Wang, C. T. Howes, M. Horányi, and S. Robertson, "Electric potentials in magnetic dipole fields normal and oblique to a surface in plasma: Understanding the solar wind interaction with lunar magnetic anomalies," Geophys. Res. Lett. **40**, 1686–1690, doi:10.1002/grl.50367 (2013).
[26]W. M. Farrell, T. J. Stubbs, J. S. Halekas, R. M. Killen, G. T. Delory, M. R. Collier, and R. R. Vondrak, "Anticipated electrical environment within permanently shadowed lunar craters," J. Geophys. Res. **115**(E3), E03004, doi:10.1029/2009je003464 (2010).
[27]M. I. Zimmerman, W. M. Farrell, T. J. Stubbs, J. S. Halekas, and T. L. Jackson, "Solar wind access to lunar polar craters: Feedback between surface charging and plasma expansion," Geophys. Res. Lett. **38**(19), L19202, doi:10.1029/2011gl048880 (2011).
[28]W. Yu, J. Wang, and K. Chou, "Laboratory measurement of lunar regolith simulant surface charging in a localized plasma wake," IEEE Trans. Plasma Sci. **43**, 4175–4181 (2015).
[29]D. A. Mendis and M. Rosenberg, "Cosmic dusty plasma," Annu. Rev. Astron. Astrophys. **32**, 419–463 (1994).
[30]M. Horányi, "Charged dust dynamics in the solar system," Annu. Rev. Astron. Astrophys. **34**, 383–418 (1996).
[31]J. J. Rennilson and D. R. Criswell, "Surveyor observations of lunar horizon-glow," Moon **10**(2), 121–142 (1974), URL: https://doi.org/10.1007/BF00655715.
[32]C. K. Goertz and G. Morfill, "A model for the formation of spokes in saturn's ring," Icarus **53**, 219–229 (1983).
[33]P. Vernazza, M. Delbo, P. L. King, M. R. M. Izawa, J. Olofsson, P. Lamy, F. Cipriani, R. P. Binzel, F. Marchis, B. Mern, and A. Tamanai, "High surface porosity as the origin of emissivity features in asteroid spectra," Icarus **221**(2), 1162–1172 (2012), URL: http://www.sciencedirect.com/science/article/pii/S0019103512001327.
[34]N. Thomas, B. Davidsson, M. R. El-Maarry, S. Fornasier, L. Giacomini, A. G. Gracia-Berná, S. F. Hviid, W.-H. Ip, L. Jorda, H. U. Keller *et al.*, "Redistribution of particles across the nucleus of comet 67p/churyumov-gerasimenko," Astron. Astrophys. **583**, A17 (2015).
[35]M. S. Robinson, P. C. Thomas, J. Veverka, S. Murchie, and B. Carcich, "The nature of ponded deposits on eros," Nature **413**(6854), 396–400 (2001), URL: https://doi.org/10.1038/35096518.
[36]X. Wang, J. Schwan, H. W. Hsu, E. Grün, and M. Horányi, "Dust charging and transport on airless planetary bodies," Geophys. Res. Lett. **43**, 6103–6110, doi:10.1002/2016GL069491 (2016).
[37]T. E. Sheridan, J. Goree, Y. T. Chiu, R. L. Rairden, and J. A. Kiessling, "Observation of dust shedding from material bodies in a plasma," J. Geophys. Res. **97**, 2935, doi:10.1029/91ja02801 (1992).
[38]B. Walch, M. Horányi, and S. Robertson, "Measurement of the charge on individual dust grains in a plasma," IEEE Trans. Plasma Sci. **22**(2), 97–102 (1994).
[39]A. A. Sickafoose, J. E. Colwell, M. Horányi, and S. Robertson, "Experimental levitation of dust grains in a plasma sheath," J. Geophys. Res. **107**(A11), 1408, doi:10.1029/2002ja009347 (2002).
[40]T. M. Flanagan and J. Goree, "Dust release from surfaces exposed to plasma," Phys. Plasmas **13**, 123504 (2006).
[41]X. Wang, J. E. Colwell, M. Horányi, and S. Robertson, "Charge of dust on surfaces in plasma," IEEE Trans. Plasma Sci. **35**(2), 271–279 (2007).
[42]X. Wang, M. Horányi, and S. Robertson, "Experiments on dust transport in plasma to investigate the origin of the lunar horizon glow," J. Geophys. Res. **114**, A05103, doi:10.1029/2008ja013983 (2009).
[43]X. Wang, M. Horányi, and S. Robertson, "Investigation of dust transport on the lunar surface in a laboratory plasma with an electron beam," J. Geophys. Res. **115**, A11102, doi:10.1029/2010ja015465 (2010).
[44]X. Wang, M. Horányi, and S. Robertson, "Dust transport near electron beam impact and shadow boundaries," Planet. Space Sci. **59**, 1791–1794 (2011).
[45]N. Ding, J. Wang, and J. Polansky, "Measurement of dust charging on a lunar regolith simulant surface," IEEE Trans. Plasma Sci. **41**, 3498–3504 (2013).
[46]C. Böhm and J. Perrin, "Retarding field analyzer for measurements of ion energy distributions and secondary electron emission coefficients in low pressure radio frequency discharges," Rev. Sci. Instrum. **64**, 31–44 (1993).
[47]Z. Sternovsky and S. Robertson, "Langmuir probe interpretation for plasmas with secondary electrons from the wall," Phys. Plasmas **11**(7), 3610–3615 (2004).

19 June 2026 00:46:47